JOURNAL OF GUIDANCE, CONTROL, AND DYNAMICS
Vol. 32, No. 1, January–February 2009

Nonlinear Adaptive Trajectory Control Applied to an F-16 Model

L. Sonneveldt,* E. R. van Oort,† Q. P. Chu,‡ and J. A. Mulder§
Delft University of Technology, 2600 GB Delft, The Netherlands

DOI: 10.2514/1.38785

A nonlinear adaptive autopilot is designed for the inertial trajectory control of a six-degree-of-freedom, high-fidelity F-16 aircraft model. The control system is decomposed in four feedback loops constructed using a single control Lyapunov function. The aerodynamic force and moment functions of the aircraft model are assumed to be unknown during the control design phase and will be approximated online. B-spline neural networks are used to partition the flight envelope into multiple connecting regions. In each partition a locally valid linear-in-the-parameters nonlinear aircraft model is defined, the unknown parameters of which are adapted online by Lyapunov-based update laws. These update laws take aircraft state and input constraints into account so that they do not corrupt the parameter-estimation process. The performance of the proposed control system has been assessed in numerical simulations of several types of trajectories at different flight conditions. Simulations with a locked control surface and uncertainties in the aerodynamic forces and moments are also included. The results demonstrate that the proposed control laws achieve closed-loop stability even in the presence of these uncertain parameters and actuator failures.

Nomenclature

b	=	wing span, m
$\bar{c}$	=	mean aerodynamic chord, m
g	=	gravity, m/s^2
h_{eng}	=	engine angular momentum about the x-body axis, kg $\cdot$ m^2/s
I_x, I_y, I_z	=	roll, pitch, and yaw moments of inertia, kg $\cdot$ m^2
I_{xz}	=	product moment of inertia, kg $\cdot$ m^2
L, Y, D	=	lift, side, and drag force components, N
$\bar{L}$, $\bar{M}$, $\bar{N}$	=	rolling, pitching, and yawing moments, N $\cdot$ m
m	=	mass, kg
p, q, r	=	body-axis roll, pitch, and yaw rates, rad/s
$\bar{q}$	=	dynamic pressure, Pa
S	=	reference wing surface area, m^2
T	=	thrust force, N
V	=	total velocity, m/s
x, y, z	=	inertial position coordinates, m
α	=	angle of attack, rad
β	=	angle of sideslip, rad
γ, χ, μ	=	flight-path, heading, and velocity roll angles, rad
δ_e, δ_a, δ_r	=	elevator, aileron, and rudder deflections, rad
δ_{LEF}	=	leading-edge flap deflection, rad
δ_t	=	throttle setting, 0–1
ϕ, θ, ψ	=	Euler angles, rad

Presented as Paper 6788 at the AIAA Guidance, Navigation, and Control Conference and Exhibit, Honolulu, HI, 19–21 August 2008; received 28 May 2008; revision received 9 September 2008; accepted for publication 9 September 2008.

*Ph.D. Student, Aerospace Software and Technology Institute, P.O. Box 5058; l.sonneveldt@tudelft.nl.

†Ph.D. Student, Aerospace Software and Technology Institute, P.O. Box 5058; e.r.vanoort@tudelft.nl.

‡Associate Professor, Control and Simulation Division, Faculty of Aerospace Engineering, P.O. Box 5058; q.p.chu@tudelft.nl.

§Professor, Chairman of the Control and Simulation Division, Faculty of Aerospace Engineering, P.O. Box 5058; j.a.mulder@tudelft.nl.

I. Introduction

IN RECENT years the advancements in microelectronics and precise navigation systems have led to an enormous rise of interest [1] in (partially) automated unmanned air vehicle (UAV) designs for a large variety of missions in both civil [2,3] and military aviation [4]. Inertial trajectory control is essential for these UAVs, because they are usually required to follow predetermined paths through certain target points in the three-dimensional air space [5–11]. Other situations in which trajectory control is desired include formation control, aerial refueling, and autonomous landing maneuvers [12–17]. This has lead to a lot of literature dedicated to formation and flight-path control for UAVs, but also for other types of manned and unmanned vehicles [18,19]. Two different approaches can be distinguished in the design of these trajectory control systems. The most popular approach is to separate the guidance and control laws: a given reference trajectory is converted by the guidance laws to velocity and attitude commands for the actual flight controller, which in turn generates the actuator signals [8,12,16]. For example, in [8] it is assumed that a flight-path-angle control autopilot exists, and a guidance law is constructed that takes heading rate and velocity constraints of the vehicle into account. The same holds for the formation control schemes of [12,16]. Usually, the assumption is made that the autopilot response to heading and airspeed commands is first order in nature to simplify the design.

The other design approach is to integrate the guidance and control laws into one system to achieve better stability guarantees and improve performance. Kaminer et al. [5] use an integrated guidance and control approach to trajectory tracking in which the trimmed flight conditions along the reference trajectory are the command input to the tracking controllers. In [7] a combination of sliding-mode control and adaptive control is used for flight-path control of an F/A-18 model.

In this paper a Lyapunov-based adaptive backstepping [20,21] approach is used to design a flight-path controller for a nonlinear high-fidelity F-16 model in three-dimensional air space. It is assumed that the aerodynamic force and moment functions of the model are not known exactly and that they can change during flight due to structural damage or control-surface failures. There is plenty of literature available on adaptive backstepping designs for the control of aircraft and missiles (see, for example, [22–29]). However, most of these designs consider control of the aerodynamic angles μ, α, and β. The design of a trajectory controller is much more complicated, because the system to be controlled is of a higher relative degree. This presents difficulties for a standard adaptive backstepping design,

because the derivatives of the intermediate control variables have to be calculated analytically in each design step. Calculating the derivatives of the intermediate control variables in each design step leads to a rapid explosion of terms. This phenomenon is the main motivation for the authors of [7] to select a sliding-mode design for the outer feedback loops: it simplifies the design considerably. Another disadvantage of standard backstepping designs (and, indeed, most feedback linearizing designs) is that the contribution of the control-surface deflections to the aerodynamic forces cannot be taken into account. For these reasons, the constrained adaptive backstepping approach of [27,29,30] is used in this paper. This method makes use of command filters to calculate the derivatives of the intermediate controls, which greatly simplifies the design. Additionally, these filters can be used to enforce magnitude and rate limits on the state and input variables so that they do not corrupt the online model-identification process.

To simplify the approximation of the unknown aerodynamic force and moment functions, the flight envelope is partitioned into multiple connecting operating regions called hyperboxes. In each hyperbox a locally valid linear-in-the-parameters nonlinear model is defined. The coefficients of these models can be estimated using the update laws of the adaptive backstepping control laws. The aerodynamic model can be partitioned using different state variables. In this study we use B-spline neural networks [31,32] to interpolate between the local nonlinear models to ensure smooth model transitions. Numerical simulations of various maneuvers with aerodynamic uncertainties in the model and actuator failures are presented. The maneuvers are performed at several flight conditions to demonstrate that the control laws are valid for the entire flight envelope. It is shown that inertia trajectory control is established for the closed-loop system even in the presence of uncertainties or failures in the aircraft model.

The paper is outlined as follows. First, the nonlinear dynamics of the aircraft model are introduced in Sec. II. In Sec. III the adaptive control design is presented decomposed in four feedback-loop designs. The identification process with the B-spline neural networks is discussed in Sec. IV. Section V validates the performance of the control laws using numerical simulations performed in MATLAB/Simulink. Finally, a summary of the results and the conclusions are given in Sec. VI.

II. Aircraft Model Description

The aircraft model used in this study is that of an F-16 fighter aircraft with geometry and aerodynamic data as reported in [33]. The aerodynamic data in tabular form have been obtained from wind-tunnel tests and are valid up to Mach 0.6 for the wide range of $-20 \text{ deg} \leq \alpha \leq 90 \text{ deg}$ and $-30 \text{ deg} \leq \beta \leq 30 \text{ deg}$. The control inputs of the model are the elevator, ailerons, rudder, and leading-edge flaps, as well as the throttle setting. The leading-edge flaps are controlled separately and will not be used for the control design. The control-surface actuators are modeled as first-order low-pass filters with rate and magnitude limits as given in [29]. Before giving the equations of motion for the F-16 model, some frame of reference in which to describe the motion is needed. The reference frames used in this paper are the Earth-fixed reference frame F_E, used as the inertial frame; the vehicle-carried local Earth reference frame F_O, with its origin fixed in the center of gravity of the aircraft, which is assumed to have the same orientation as F_E; the wind-axes reference frame F_W, obtained from F_O by three successive rotations of χ, γ, and μ; the stability-axes reference frame F_S, obtained from F_W by a rotation of $-\beta$; and the body-fixed reference frame F_B, obtained from F_S by a rotation of α, as is also indicated in Fig. 1. The body-fixed reference frame F_B can also be obtained directly from F_O by three successive rotations of yaw angle ψ, pitch angle θ, and roll angle ϕ. More details and transformation matrices are given in, for example, [34,35]. Assuming that the aircraft has a rigid body, which is symmetric around the X–Z body-fixed plane, the relevant nonlinear coupled equations of motion can described by [34]

$$\dot{X}_0 = \begin{bmatrix} V\cos\chi\cos\gamma \\ V\sin\chi\cos\gamma \\ -V\sin\gamma \end{bmatrix} \tag{1}$$

$$\dot{X}_1 = \begin{bmatrix} \frac{1}{m}(-D + T\cos\alpha\cos\beta) - g\sin\gamma \\ \frac{1}{mV\cos\gamma}(L\sin\mu + Y\cos\mu + T(\sin\alpha\sin\mu - \cos\alpha\sin\beta\cos\mu)) \\ \frac{1}{mV}(L\cos\mu - Y\sin\mu + T(\cos\alpha\sin\beta\sin\mu + \sin\alpha\cos\mu)) - \frac{g}{V}\cos\gamma \end{bmatrix} \tag{2}$$

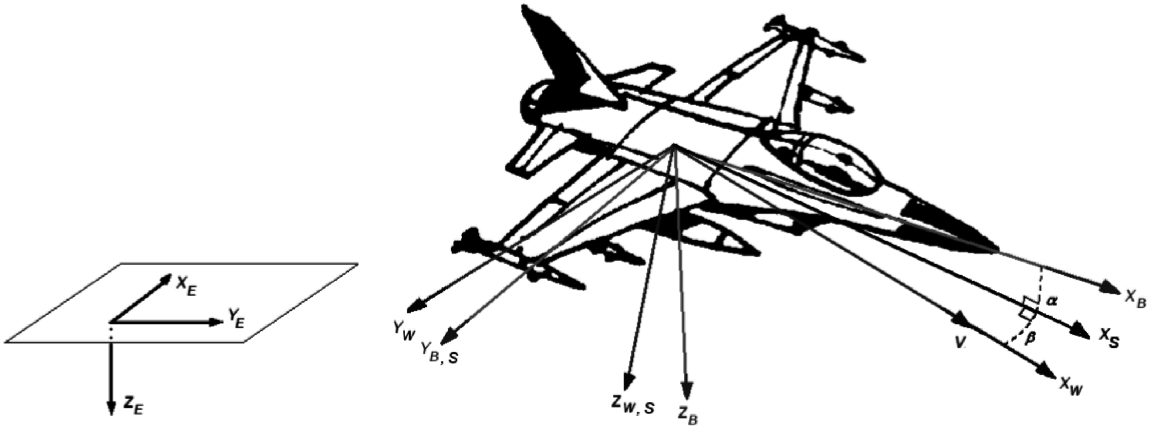

Fig. 1 Aircraft reference frames.

$$\dot{X}_2 = \begin{bmatrix} \frac{\cos\alpha}{\cos\beta} & 0 & \frac{\sin\alpha}{\cos\beta} \\ -\cos\alpha\tan\beta & 1 & -\sin\alpha\tan\beta \\ \sin\alpha & 0 & -\cos\alpha \end{bmatrix} X_3 + \begin{bmatrix} 0 & \sin\gamma + \cos\gamma\sin\mu\tan\beta & \cos\mu\tan\beta \\ 0 & -\frac{\cos\gamma\sin\mu}{\cos\beta} & -\frac{\cos\mu}{\cos\beta} \\ 0 & \cos\gamma\cos\mu & -\sin\mu \end{bmatrix} \dot{X}_1 \tag{3}$$

$$\dot{X}_3 = \begin{bmatrix} (c_1 r + c_2 p)q + c_3\bar{L} + c_4(\bar{N} + h_e q) \\ c_5 pr - c_6(p^2 - r^2) + c_7(\bar{M} - h_e r) \\ (c_8 p - c_2 r)q + c_4\bar{L} + c_9(\bar{N} + h_e q) \end{bmatrix} \tag{4}$$

where $X_0 = (x, y, z)^T$, $X_1 = (V, \chi, \gamma)^T$, $X_2 = (\mu, \alpha, \beta)^T$, $X_3 = (p, q, r)^T$, and the definition of the inertia terms c_i $(i = 1, \ldots, 9)$ is given in, for example, [29]. The engine angular momentum h_e is assumed to be constant. These 12 differential equations are sufficient to describe the complete motion of the aircraft; other states such as the attitude angles ϕ, θ, and ψ are functions of $X = (X_0^T, X_1^T, X_2^T, X_3^T)^T$, and their dynamics can be expressed as

$$\dot{\phi} = p + (q\sin\phi + r\cos\phi)\tan\theta, \qquad \dot{\theta} = q\cos\phi - r\sin\phi$$
$$\dot{\psi} = \frac{q\sin\phi + r\cos\phi}{\cos\theta} \tag{5}$$

The thrust model of [33] is implemented, which calculates the thrust as a function of altitude, Mach number, and throttle setting δ_t. This model is given in tabular form. The total aerodynamic forces L, Y, and D (expressed in F_W) and moments $\bar{L}$, $\bar{M}$, and $\bar{N}$ (expressed in F_B) are summations of the various aerodynamic contributions stored in lookup tables. As an example, the total pitch moment $\bar{M}$ is given by

$$\bar{M} = \bar{q}S\bar{c}\Bigg(C_m(\alpha, \beta, \delta_e) + C_{Z_T}[x_{cg_r} - x_{cg}] + \delta C_{m_{\text{LEF}}}\left(1 - \frac{\delta_{\text{LEF}}}{25}\right) + \frac{q\bar{c}}{2V_T}[C_{m_q}(\alpha) + \delta C_{m_{q_{\text{LEF}}}}(\alpha)]\left(1 - \frac{\delta_{\text{LEF}}}{25}\right) + \delta C_m(\alpha) + \delta C_{m_{ds}}(\alpha, \delta_e)\Bigg) \tag{6}$$

Other aerodynamic forces and moments are given in similar form; for a detailed discussion, see [33].

III. Adaptive Control Design

In this section we aim to develop an adaptive guidance and control system that asymptotically tracks a smooth prescribed inertial trajectory $Y^{\text{ref}} = (x^{\text{ref}}, y^{\text{ref}}, z^{\text{ref}})^T$ with position states $X_0 = (x, y, z)^T$. Furthermore, the sideslip angle β has to be kept at zero to enable coordinated turning. It is assumed that the reference trajectory $Y^{\text{ref}} = (x^{\text{ref}}, y^{\text{ref}}, z^{\text{ref}})^T$ satisfies

$$\dot{x}^{\text{ref}} = V^{\text{ref}}\cos\chi^{\text{ref}} \tag{7}$$

$$\dot{y}^{\text{ref}} = V^{\text{ref}}\sin\chi^{\text{ref}} \tag{8}$$

with V^{ref}, χ^{ref}, z^{ref}, and their derivatives continuous and bounded. It also assumed that the components of the total aerodynamic forces L, Y, and D and moments $\bar{L}$, $\bar{M}$, and $\bar{N}$ are uncertain, and so these will have to be estimated. The available controls are the control-surface deflections $(\delta_e, \delta_a, \delta_r)^T$ and the engine thrust T. The Lyapunov-based control design based on [27,29] is done in four feedback loops, starting at the outer loop.

A. Inertial Position Control

We start the outer-loop feedback control design by transforming the tracking control problem into a regulation problem:

$$Z_0 = \begin{bmatrix} z_{01} \\ z_{02} \\ z_{03} \end{bmatrix} = \begin{bmatrix} \cos\chi & \sin\chi & 0 \\ -\sin\chi & \cos\chi & 0 \\ 0 & 0 & 1 \end{bmatrix}(X_0 - Y^{\text{ref}}) \tag{9}$$

where we introduce a new rotating reference frame for control that is fixed to the aircraft and aligned with the horizontal component of the velocity vector [8,13]. Differentiating Eq. (9) now gives

$$\dot{Z}_0 = \begin{bmatrix} V + z_{02}\dot{\chi} - V^{\text{ref}}\cos(\chi - \chi^{\text{ref}}) \\ -z_{01}\dot{\chi} + V^{\text{ref}}\sin(\chi - \chi^{\text{ref}}) \\ \dot{z}^{\text{ref}} - V\sin\gamma \end{bmatrix} \tag{10}$$

We want to control the position errors Z_0 through the flight-path angles χ and γ and the total airspeed V. However, from Eq. (10) it is clear that it is not yet possible to do something about z_{02} in this design step. We select the virtual controls

$$V^{\text{des},0} = V^{\text{ref}}\cos(\chi - \chi^{\text{ref}}) - c_{01}z_{01} \tag{11}$$

$$\gamma^{\text{des},0} = \arcsin\left(\frac{c_{03}z_{03} - \dot{z}^{\text{ref}}}{V}\right), \qquad -\pi/2 < \gamma < \pi/2 \tag{12}$$

where c_{01} and $c_{03} > 0$ are the control gains. The actual implementable virtual control signals V^{des} and γ^{des}, as well as their derivatives $\dot{V}^{\text{des}}$ and $\dot{\gamma}^{\text{des}}$, are obtained by filtering the virtual signals with a second-order low-pass filter. In this way, tedious calculation of the virtual control derivatives is avoided [36]. An additional advantage is that the filters can be used to enforce magnitude or rate limits on the states [24,27]. As an example, the state-space representation of such a filter for $V^{\text{des},0}$ is given by

$$\begin{bmatrix} \dot{q}_1(t) \\ \dot{q}_2(t) \end{bmatrix} = \begin{bmatrix} q_2 \\ 2\zeta_V\omega_V(S_R(\frac{\omega_V^2}{2\zeta_V\omega_V}[S_M(V^{\text{des},0}) - q_1]) - q_2) \end{bmatrix} \tag{13}$$

$$\begin{bmatrix} V^{\text{des}} \\ \dot{V}^{\text{des}} \end{bmatrix} = \begin{bmatrix} q_1 \\ q_2 \end{bmatrix} \tag{14}$$

where $S_M(.)$ and $S_R(.)$ represent the magnitude and rate limit functions as given in [27]. These functions enforce the state V to stay within the defined limits. Note that if the signal $V^{\text{des},0}$ is bounded, then V^{des} and $\dot{V}^{\text{des}}$ are also bounded and continuous signals. When the magnitude and rate limits are not in effect, the transfer function from $V^{\text{des},0}$ to V^{des} is given by

$$\frac{V^{\text{des}}(s)}{V^{\text{des},0}(s)} = \frac{\omega_v^2}{s^2 + 2\zeta_v\omega_v + \omega_v^2} \tag{15}$$

and the error $V^{\text{des},0} - V^{\text{des}}$ can be made arbitrarily small by selecting the bandwidth of the filter to be sufficiently large [36].

B. Flight-Path Angle and Airspeed Control

In this loop the objective is to steer V and γ to their desired values, as determined in the previous section. Furthermore, the heading angle χ has to track the reference signal χ^{ref}, and we also have to make sure that z_{02} is regulated to zero. The available (virtual) controls in this step are the aerodynamic angles μ and α, as well as the thrust T. The lift, drag, and side forces are assumed to be unknown and will be estimated. Note that the aerodynamic forces also depend on the control-surface deflections $U = (\delta_e, \delta_a, \delta_r)^T$. These forces are quite small, because the surfaces are primarily moment generators. However, because the current control-surface deflections are available from the command filters used in the inner loop, we can take them into account in the control design. The relevant equations of motion are given by

$$\dot{X}_1 = A_1 F_1(X,U) + B_1 G_1(X,U,X_2) + H_1(X) \tag{16}$$

where

$$A_1 = \frac{1}{mV}\begin{bmatrix} 0 & 0 & -V \\ 0 & \frac{\cos\mu}{\cos\gamma} & 0 \\ 0 & -\sin\mu & 0 \end{bmatrix}$$

$$H_1 = \begin{bmatrix} -g\sin\gamma \\ \frac{T}{mV\cos\gamma}\cos\alpha\sin\beta\cos\mu \\ \frac{T}{mV}\cos\alpha\sin\beta\sin\mu - \frac{g}{V}\cos\gamma \end{bmatrix}$$

$$B_1 = \frac{1}{mV}\begin{bmatrix} V\cos\alpha\cos\beta & 0 & 0 \\ 0 & \frac{1}{\cos\gamma} & 0 \\ 0 & 0 & 1 \end{bmatrix}$$

are known (matrix) functions, and

$$F_1 = \begin{bmatrix} L(X,U) \\ Y(X,U) \\ D(X,U) \end{bmatrix}, \qquad G_1 = \begin{bmatrix} T \\ (L(X,U) + T\sin\alpha)\sin\mu \\ (L(X,U) + T\sin\alpha)\cos\mu \end{bmatrix}$$

are functions containing the uncertain aerodynamic forces. Note that the intermediate control variables α and μ do not appear affine in the X_1 subsystem, which complicates the design somewhat. Because the control objective in this step is to track the smooth reference signal $X_1^{\text{des}} = (V^{\text{des}}, \chi^{\text{ref}}, \gamma^{\text{des}})^T$ with $X_1 = (V, \chi, \gamma)^T$, the tracking errors are defined as

$$Z_1 = \begin{bmatrix} z_{11} \\ z_{12} \\ z_{13} \end{bmatrix} = X_1 - X_1^{\text{des}} \tag{17}$$

To regulate Z_1 *and* z_{02} to zero, the following equation needs to be satisfied [37]:

$$B_1\hat{G}_1(X,U,X_2) = \begin{bmatrix} -c_{11}z_{11} \\ -V^{\text{ref}}(c_{02}z_{02} + c_{12}\sin z_{12}) \\ -c_{13}z_{13} \end{bmatrix} - A_1\hat{F}_1 - H_1 + \dot{X}_1^{\text{des}} \tag{18}$$

where $\hat{F}_1$ is the estimate of F_1 and where

$$\hat{G}_1(X,U,X_2) = \begin{bmatrix} T \\ (\hat{L}_0(X,U) + \hat{L}_\alpha(X,U)\alpha + T\sin\alpha)\sin\mu \\ (\hat{L}_0(X,U) + \hat{L}_\alpha(X,U)\alpha + T\sin\alpha)\cos\mu \end{bmatrix} \tag{19}$$

with the estimate of the lift force decomposed as

$$\hat{L}(X,U) = \hat{L}_0(X,U) + \hat{L}_\alpha(X,U)\alpha$$

The estimate of the aerodynamic forces $\hat{F}_1$ is defined as

$$\hat{F}_1 = \Phi_{F_1}^T(X,U)\hat{\Theta}_{F_1} \tag{20}$$

where $\Phi_{F_1}^T$ is the known regressor function and $\hat{\Theta}_{F_1}$ is a vector with unknown constant parameters. It is assumed that there exists a vector Θ_{F_1} such that

$$F_1 = \Phi_{F_1}^T(X,U)\Theta_{F_1} \tag{21}$$

This means the estimation error can be defined as $\tilde{\Theta}_{F_1} = \Theta_{F_1} - \hat{\Theta}_{F_1}$. We now need to determine the desired values α^{des} and μ^{des}. The right-hand side of Eq. (18) is entirely known, and so the left-hand side can be determined and the desired values can be extracted. This is done by introducing the coordinate transformation

$$x \equiv (\hat{L}_0(X,U) + \hat{L}_\alpha(X,U)\alpha + T\sin\alpha)\cos\mu \tag{22}$$

$$y \equiv (\hat{L}_0(X,U) + \hat{L}_\alpha(X,U)\alpha + T\sin\alpha)\sin\mu \tag{23}$$

which can be seen as a transformation from the two-dimensional polar coordinates

$$(\hat{L}_0(X,U) + \hat{L}_\alpha(X,U)\alpha + T\sin\alpha)$$

and μ to Cartesian coordinates x and y. The desired signals $(T^{\text{des},0}, y_0, x_0)^T$ are given by

$$B_1\begin{bmatrix} T^{\text{des},0} \\ y_0 \\ x_0 \end{bmatrix} = \begin{bmatrix} -c_{11}z_{11} \\ -V^{\text{ref}}(c_{02}z_{02} + c_{12}\sin z_{12}) \\ -c_{13}z_{13} \end{bmatrix} - A_1\hat{F}_1 - H_1 + \dot{X}_1^{\text{des}} \tag{24}$$

Thus, the virtual control signals are equal to

$$\hat{L}_\alpha(X,U)\alpha^{\text{des},0} = \sqrt{x_0^2 + y_0^2} - \hat{L}_0(X,U) - T\sin\alpha \tag{25}$$

and

$$\mu^{\text{des},0} = \begin{cases} \arctan(\frac{y_0}{x_0}) & \text{if } x_0 > 0 \\ \arctan(\frac{y_0}{x_0}) + \pi & \text{if } x_0 < 0 \quad \text{and} \quad y_0 \geq 0 \\ \arctan(\frac{y_0}{x_0}) - \pi & \text{if } x_0 < 0 \quad \text{and} \quad y_0 < 0 \\ \frac{\pi}{2} & \text{if } x_0 = 0 \quad \text{and} \quad y_0 > 0 \\ -\frac{\pi}{2} & \text{if } x_0 = 0 \quad \text{and} \quad y_0 < 0 \end{cases} \tag{26}$$

Filtering the virtual signals to account for magnitude, rate, and bandwidth limits will give the implementable virtual controls α^{des} and μ^{des} and their derivatives. The sideslip-angle command was already defined as $\beta^{\text{ref}} = 0$, and thus $X_2^{\text{des}} = (\mu^{\text{des}}, \alpha^{\text{des}}, 0)^T$ and its derivative are completely defined. However, care must be taken because the desired virtual control $\mu^{\text{des},0}$ is undefined when both x_0 and y_0 are equal to zero, making the system momentarily uncontrollable. This sign change of

$$(\hat{L}_0(X,U) + \hat{L}_\alpha(X,U)\alpha + T\sin\alpha)$$

can only occur at very low or negative angles of attack. This situation was not encountered during the maneuvers simulated in this study. To solve the problem altogether, the designer could measure the rate of change for x_0 and y_0 and devise a rule base set to change sign when these terms approach zero. Furthermore, problems will also occur at high angles of attack when the control effectiveness term $\hat{L}_\alpha$ will become smaller and eventually change sign. Possible solutions include limiting the angle-of-attack commands using the command filters or proper trajectory planning to avoid high-angle-of-attack maneuvers. Also note that so far in the control design process, we have not taken care of the update laws for the uncertain aerodynamic forces; they will be dealt with when the static control design is finalized.

C. Aerodynamic Angle Control

Now that the reference signal $X_2^{\text{des}} = (\mu^{\text{des}}, \alpha^{\text{des}}, \beta^{\text{ref}})^T$ and its derivative have been found, we can move on to the next feedback loop. The available virtual controls in this step are the angular rates X_3. The relevant equations of motion for this part of the design are given by

$$\dot{X}_2 = A_2 F_1(X,U) + B_2(X)X_3 + H_2(X) \tag{27}$$

where

$$A_2 = \frac{1}{mV}\begin{bmatrix} (\tan\beta + \tan\gamma\sin\mu) & \tan\gamma\cos\mu & 0 \\ \frac{-1}{\cos\beta} & 0 & 0 \\ 0 & 1 & 0 \end{bmatrix} \qquad B_2 = \begin{bmatrix} \frac{\cos\alpha}{\cos\beta} & 0 & \frac{\sin\alpha}{\cos\beta} \\ -\cos\alpha\tan\beta & 1 & -\sin\alpha\tan\beta \\ \sin\alpha & 0 & \cos\alpha \end{bmatrix}$$

$$H_2 = \frac{1}{mV}\begin{bmatrix} T(\sin\alpha\tan\gamma\sin\mu + \sin\alpha\tan\beta - \cos\alpha\sin\beta\tan\gamma\cos\mu) - \frac{g}{V}\tan\beta\cos\gamma\cos\mu \\ T\frac{\sin\alpha}{\cos\beta} + \frac{g}{V}\cos\gamma\cos\mu \\ -T\cos\alpha\cos\beta + \frac{g}{V}\cos\gamma\sin\mu \end{bmatrix}$$

are known (matrix) functions. The tracking errors are defined as

$$Z_2 = X_2 - X_2^{\text{des}} \tag{28}$$

To stabilize the Z_2 subsystem, a virtual feedback control $X_3^{\text{des},0}$ is defined as

$$B_2 X_3^{\text{des},0} = -C_2 Z_2 - A_2\hat{F}_1 - H_2 + \dot{X}_2^{\text{des}}, \qquad C_2 = C_2^T > 0 \tag{29}$$

The implementable virtual control (i.e., the reference signal for the inner loop) X_3^{des} and its derivative are again obtained by filtering the virtual control signal $X_3^{\text{des},0}$ with a second-order command-limiting filter.

D. Angular Rate Control

In the fourth step, an inner-loop feedback loop for the control of the body-axis angular rates $X_3 = (p, q, r)^T$ is constructed. The control inputs for the inner loop are the control-surface deflections $U = (\delta_e, \delta_a, \delta_r)^T$. The dynamics of the angular rates can be written as

$$\dot{X}_3 = A_3(F_3(X, U) + B_3(X)U) + H_3(X) \tag{30}$$

where

$$A_3 = \begin{bmatrix} c_3 & 0 & c_4 \\ 0 & c_7 & 0 \\ c_4 & 0 & c_9 \end{bmatrix}, \qquad H_3 = \begin{bmatrix} (c_1 r + c_2 p)q \\ c_5 pr - c_6(p^2 - r^2) \\ (c_8 p - c_2 r)q \end{bmatrix}$$

are known (matrix) functions, and

$$F_3 = \begin{bmatrix} \bar{L}_0 \\ \bar{M}_0 \\ \bar{N}_0 \end{bmatrix}, \qquad B_3 = \begin{bmatrix} \bar{L}_{\delta_e} & \bar{L}_{\delta_a} & \bar{L}_{\delta_r} \\ \bar{M}_{\delta_e} & \bar{M}_{\delta_a} & \bar{M}_{\delta_r} \\ \bar{N}_{\delta_e} & \bar{N}_{\delta_a} & \bar{N}_{\delta_r} \end{bmatrix}$$

are unknown (matrix) functions that have to be approximated. Note that for a more convenient presentation, the aerodynamic moments have been decomposed: for example,

$$\bar{M}(X, U) = \bar{M}_0(X, U) + \bar{M}_{\delta_e}\delta_e + \bar{M}_{\delta_a}\delta_a + \bar{M}_{\delta_r}\delta_r \tag{31}$$

where the higher-order control-surface dependencies are still contained in $\bar{M}_0(X, U)$. The control objective in this feedback loop is to track the reference signal $X_3^{\text{des}} = (p^{\text{ref}}, q^{\text{ref}}, r^{\text{ref}})^T$ with the angular rates X_3. Defining the tracking errors

$$Z_3 = X_3 - X_3^{\text{des}} \tag{32}$$

and taking the derivatives results in

$$\dot{Z}_3 = A_3(F_3(X, U) + B_3(X)U) + H_3(X) - \dot{X}_3^{\text{des}} \tag{33}$$

To stabilize the system of Eq. (33), we define the desired control U^0 as

$$A_3\hat{B}_3 U^0 = -C_3 Z_3 - A_3\hat{F}_3 - H_3 + \dot{X}_3^{\text{des}}, \qquad C_3 = C_3^T > 0 \tag{34}$$

where $\hat{F}_3$ and $\hat{B}_3$ are the estimates of the unknown nonlinear aerodynamic moment functions F_3 and B_3, respectively. The F-16 model is not overactuated (i.e., the B_3 matrix is square). If this is not the case, some form of control allocation would be required [38,39]. The estimates are defined as

$$\hat{F}_3 = \Phi_{F_3}^T(X, U)\hat{\Theta}_{F_3}, \qquad \hat{B}_{3i} = \Phi_{B_{3i}}^T(X)\hat{\Theta}_{B_{3i}} \quad \text{for } i = 1, \ldots, 3 \tag{35}$$

where $\Phi_{F_3}^T$ and $\Phi_{B_{3i}}^T$ are the known regressor functions, $\hat{\Theta}_{F_3}$ and $\hat{\Theta}_{B_{3i}}$ are vectors with unknown constant parameters, and $\hat{B}_{3i}$ represents the ith column of $\hat{B}_3$. It is assumed that there exist vectors Θ_{F_3} and $\Theta_{B_{3i}}$ such that

$$F_3 = \Phi_{F_3}^T(X, U)\Theta_{F_3}, \qquad B_{3i} = \Phi_{B_{3i}}^T(X)\Theta_{B_{3i}} \tag{36}$$

This means the estimation errors can be defined as $\tilde{\Theta}_{F_3} = \Theta_{F_3} - \hat{\Theta}_{F_3}$ and $\tilde{\Theta}_{B_{3i}} = \Theta_{B_{3i}} - \hat{\Theta}_{B_{3i}}$. The actual control U is found by applying a filter similar to Eq. (13) to U^0.

E. Update Laws and Stability Properties

We have now finished the static part of our control design. In this section the stability properties of the control law are discussed and dynamic update laws for the unknown parameters are derived. Define the control Lyapunov function

$$\begin{aligned} V = \frac{1}{2}\Bigg(& Z_0^T Z_0 + z_{11}^2 + \frac{2 - 2\cos z_{12}}{c_{02}} + z_{13}^2 + Z_2^T Z_2 + Z_3^T Z_3 \Bigg) \\ & + \frac{1}{2}\Bigg(\text{trace}\Big(\tilde{\Theta}_{F_1}^T \Gamma_{F_1}^{-1}\tilde{\Theta}_{F_1}\Big) + \text{trace}\Big(\tilde{\Theta}_{F_3}^T \Gamma_{F_3}^{-1}\tilde{\Theta}_{F_3}\Big) \\ & + \sum_{i=1}^{3} \text{trace}\Big(\tilde{\Theta}_{B_{3i}}^T \Gamma_{B_{3i}}^{-1}\tilde{\Theta}_{B_{3i}}\Big)\Bigg) \end{aligned} \tag{37}$$

with the update gains matrices $\Gamma_{F_1} = \Gamma_{F_1}^T > 0$, $\Gamma_{F_3} = \Gamma_{F_3}^T > 0$, and $\Gamma_{B_{3i}} = \Gamma_{B_{3i}}^T > 0$. Taking the derivative of V along the trajectories of the closed-loop system gives

$$\begin{aligned} \dot{V} = & -c_{01}z_{01}^2 + z_{02}z_{01}\dot{\chi} + (V - V^{\text{des},0})z_{01} \\ & + z_{02}(-z_{01}\dot{\chi} + V^{\text{ref}}\sin z_{12}) - c_{03}z_{03}^2 - V(\sin\gamma - \sin\gamma^{\text{des},0})z_{03} \\ & - c_{11}z_{11}^2 - V^{\text{ref}}\Bigg(\sin z_{12}z_{02} + \frac{c_{12}}{c_{02}}\sin^2 z_{12}\Bigg) - c_{13}z_{13}^2 \\ & + Z_1^T(A_1\Phi_{F_1}^T\tilde{\Theta}_{F_1} + B_1(G_1(X_2) - \hat{G}_1(X_2))) \\ & + Z_1^T B_1\Big(\hat{G}_1(X_2) - \hat{G}_1\Big(X_2^{\text{des},0}\Big)\Big) - Z_2^T C_2 Z_2 + Z_2^T A_2\Phi_{F_1}^T\tilde{\Theta}_{F_1} \\ & + Z_2^T B_2\Big(X_3 - X_3^{\text{des},0}\Big) - Z_3^T C_3 Z_3 \\ & + Z_3^T A_3\Bigg(\Phi_{F_3}^T\tilde{\Theta}_{F_3} + \sum_{i=1}^{3}\Phi_{B_{3i}}^T\tilde{\Theta}_{B_{3i}}U_i\Bigg) + Z_3^T A_3\hat{B}_3(U - U^0) \\ & - \text{trace}\Big(\dot{\hat{\Theta}}_{F_1}^T\Gamma_{F_1}^{-1}\tilde{\Theta}_{F_1}\Big) - \text{trace}\Big(\dot{\hat{\Theta}}_{F_3}^T\Gamma_{F_3}^{-1}\tilde{\Theta}_{F_3}\Big) \\ & - \sum_{i=1}^{3}\text{trace}\Big(\dot{\hat{\Theta}}_{B_{3i}}^T\Gamma_{B_{3i}}^{-1}\tilde{\Theta}_{B_{3i}}\Big) \end{aligned} \tag{38}$$

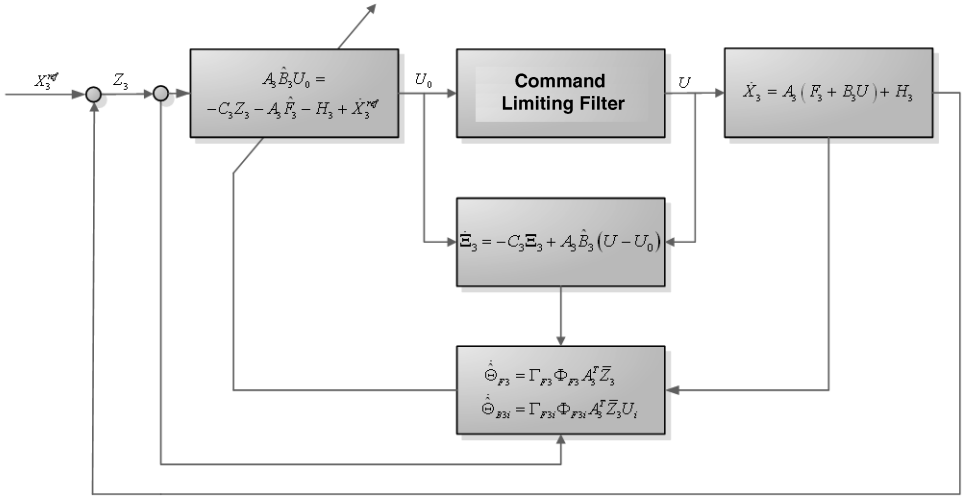

Fig. 2 Inner-loop control system.

To cancel the terms in Eq. (38), depending on the estimation errors, we select the update laws

$$\dot{\hat{\Theta}}_{F_1} = \Gamma_{F_1}\Phi_{F_1}\left(A_{1a}^T Z_1 + A_2^T Z_2\right), \qquad \dot{\hat{\Theta}}_{F_3} = \Gamma_{F_3}\Phi_{F_3}A_3^T Z_3$$
$$\dot{\hat{\Theta}}_{B_{3i}} = \mathrm{proj}_{B_{3i}}\left(\Gamma_{B_{3i}}\Phi_{B_{3i}}A_3^T Z_3 U_i\right) \tag{39}$$

with

$$A_{1a}\Phi_{F_1}^T\tilde{\Theta}_{F_1} = A_1\Phi_{F_1}^T\tilde{\Theta}_{F_1} + B_1(G_1(X_2) - \hat{G}_1(X_2))$$

The update laws for $\hat{B}_3$ include a projection operator [40] to ensure that certain elements of the matrix do not change sign and full rank is maintained always. For most elements, the sign is known based on physical principles. Substituting the update laws in Eq. (38) leads to

$$\begin{aligned}\dot{V} = {} & -c_{01}z_{01}^2 - c_{03}z_{03}^2 - c_{11}z_{11}^2 - V^{\mathrm{ref}}\frac{c_{12}}{c_{02}}\sin^2 z_{12} - c_{13}z_{13}^2 \\ & - Z_2^T C_2 Z_2 - Z_3^T C_3 Z_3 + (V - V^{\mathrm{des},0})z_{01} \\ & - V(\sin\gamma - \sin\gamma^{\mathrm{des},0})z_{03} + Z_1^T B_1\left(\hat{G}_1(X_2) - \hat{G}_1\left(X_2^{\mathrm{des},0}\right)\right) \\ & + Z_2^T B_2\left(X_3 - X_3^{\mathrm{des},0}\right) + Z_3^T A_3\hat{B}_3(U - U^0)\end{aligned} \tag{40}$$

where the first line is already negative semidefinite, which we need to prove stability in the sense of Lyapunov. Because our Lyapunov function V equation (37) is not radially unbounded, we can only guarantee local asymptotic stability [37]. This is sufficient for our operating area if we properly initialize the control law to ensure $z_{12} \leq \pm\pi/2$. However, we also have indefinite error terms due to the tracking errors and due to the command filters used in the design. As mentioned before, when no rate or magnitude limits are in effect, the difference between the input and output of the filters can be made small by selecting the bandwidth of the filters to be sufficiently larger than the bandwidth of the input signal. Also, when no limits are in effect and the small bounded difference between the input and output of the command filters is neglected, the feedback controller designed in the previous sections will converge the tracking errors to zero (for proof, see [27,29,30]).

Naturally, when control or state limits are in effect, the system will in general not track the reference signal asymptotically. A problem with adaptive control is that this can lead to corruption of the parameter-estimation process, because the tracking errors that are driving this process are no longer caused by the function approximation errors alone [24]. To solve this problem we will use a modified definition of the tracking errors in the update laws in which the effect of the magnitude and rate limits has been removed, as suggested in [27,28]. Define the modified tracking errors

$$\bar{Z}_1 = Z_1 - \Xi_1, \qquad \bar{Z}_2 = Z_2 - \Xi_2, \qquad \bar{Z}_3 = Z_3 - \Xi_3 \tag{41}$$

with the linear filters

$$\begin{aligned}\dot{\Xi}_1 &= -C_1\Xi_1 + B_1\left(\hat{G}_1(X, U, X_2) - \hat{G}_1\left(X, U, X_2^{\mathrm{des},0}\right)\right) \\ \dot{\Xi}_2 &= -C_2\Xi_2 + B_2\left(X_3 - X_3^{\mathrm{des},0}\right) \\ \dot{\Xi}_3 &= -C_3\Xi_3 + A_3\hat{B}_3(U - U^0)\end{aligned} \tag{42}$$

The modified errors will still converge to zero when the constraints are in effect, which means the robustified update laws look like

$$\dot{\hat{\Theta}}_{F_1} = \Gamma_{F_1}\Phi_{F_1}\left(A_{1a}^T\bar{Z}_1 + A_2^T\bar{Z}_2\right), \qquad \dot{\hat{\Theta}}_{F_3} = \Gamma_{F_3}\Phi_{F_3}A_3^T\bar{Z}_3$$
$$\dot{\hat{\Theta}}_{B_{3i}} = \mathrm{Proj}_{B_{3i}}\left(\Gamma_{B_{3i}}\Phi_{B_{3i}}A_3^T\bar{Z}_3 U_i\right) \tag{43}$$

To better illustrate the structure of the control system, a scheme of the adaptive inner-loop controller is shown in Fig. 2.

IV. Model Identification

To simplify the approximation of the unknown aerodynamic force and moment functions, thereby reducing computational load, the flight envelope is partitioned into multiple connecting operating regions called *hyperboxes* or *clusters*. This can be done manually using a priori knowledge of the nonlinearity of the system, automatically using nonlinear optimization algorithms that cluster the data into hyperplanar or hyperellipsoidal clusters [41] or a combination of both. In each hyperbox a locally valid linear-in-the-parameters nonlinear model is defined, which can be estimated using

Table 1 Command-filter parameters

Command variable	ω_n, rad/s	Magnitude limit	Rate limit
V^{des}	5	——	——
γ^{des}	3	±80 deg	——
μ^{des}	8	±80 deg	——
α^{des}	8	——	——
p^{des}	20	——	——
q^{des}	20	——	——
r^{des}	10	——	——
δ_e	40.4	±25 deg	±60 deg/s
δ_a	40.4	±21.5 deg	±80 deg/s
δ_r	40.4	±30 deg	±120 deg/s
T	10	[1000–100,000] N	±40,000 N/s

the update laws of the Lyapunov-based control laws. The aerodynamic model can be partitioned using different state variables, the choice of which depends on the expected nonlinearities of the system. In this study we use B-spline neural networks [31,32] (i.e., radial basis function neural networks with B-spline basis functions) to interpolate between the local nonlinear models, ensuring smooth transitions. In the previous section we defined parameter update laws equation (43) for the unknown aerodynamic functions, which were written as

$$\hat{F}_1 = \Phi^T_{F_1}(X,U)\hat{\Theta}_{F_1}, \qquad \hat{F}_3 = \Phi^T_{F_3}(X,U)\hat{\Theta}_{F_3}$$
$$\hat{B}_{3i} = \Phi^T_{B_{3i}}(X)\hat{\Theta}_{B_{3i}} \tag{44}$$

Now we will further define these unknown vectors and known regressor vectors. The total force approximations are defined as

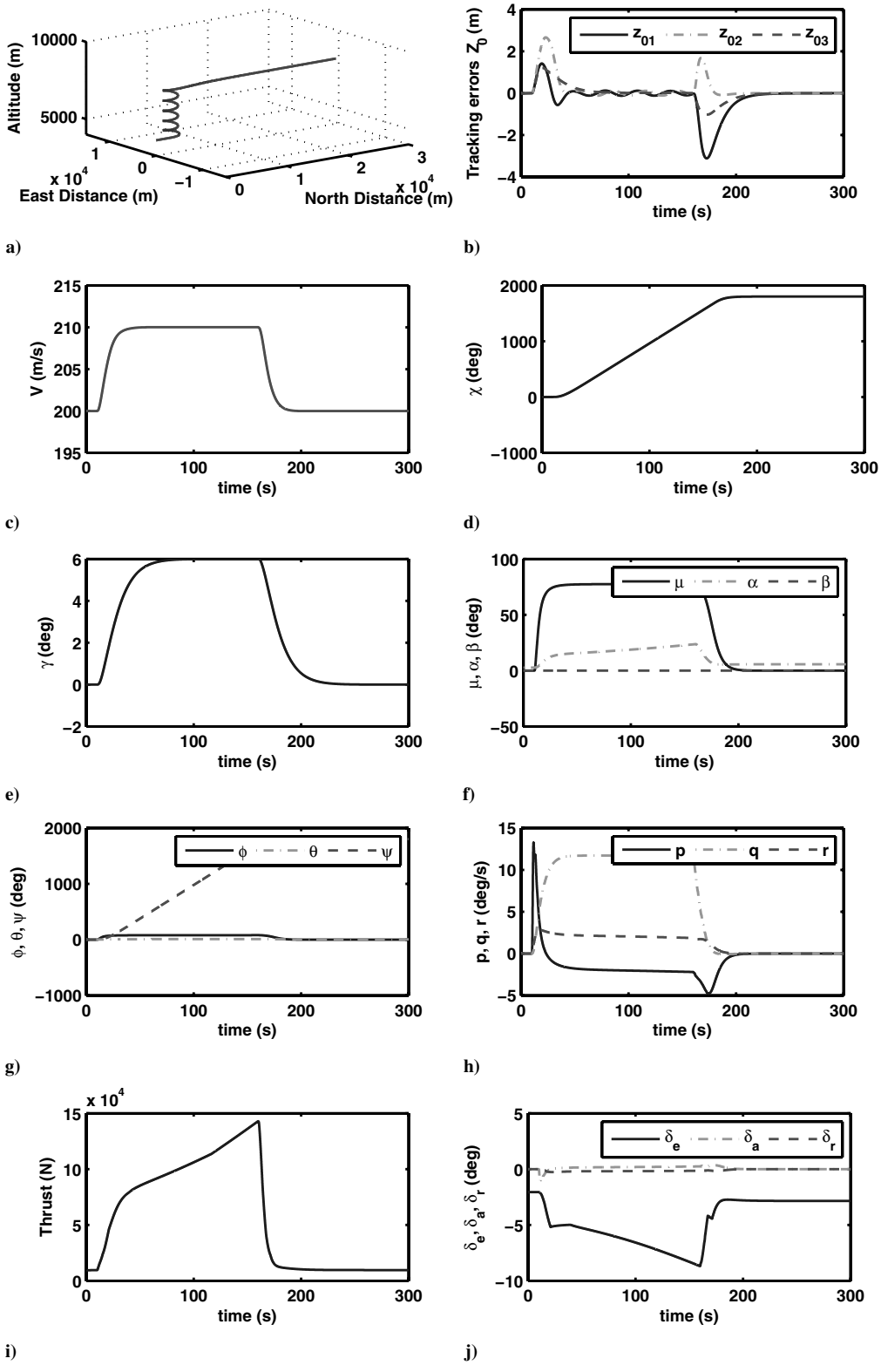

Fig. 3 Maneuver 1: climbing helical path performed at flight condition 1 without any uncertainty or actuator failures.

$$\hat{L} = \bar{q}S\left(\hat{C}_{L_0}(\alpha,\beta) + \hat{C}_{L_\alpha}(\beta,\delta_e)\alpha + \hat{C}_{L_q}(\alpha)\frac{q\bar{c}}{2V} + \hat{C}_{L_{\delta_e}}(\alpha,\beta)\delta_e\right)$$
$$\hat{Y} = \bar{q}S\left(\hat{C}_{Y_0}(\alpha,\beta,\delta_e) + \hat{C}_{Y_p}(\alpha,\beta)\frac{pb}{2V} + \hat{C}_{Y_r}(\alpha,\beta)\frac{rb}{2V} + \hat{C}_{Y_{\delta_a}}(\alpha,\beta)\delta_a + \hat{C}_{Y_{\delta_r}}(\alpha,\beta)\delta_r\right)$$
$$\hat{D} = \bar{q}S(\hat{C}_{D_0}(\alpha,\beta,\delta_e) + \hat{C}_{D_{\delta_e}}(\alpha,\beta)\delta_e) \tag{45}$$

and the moment approximations are defined as

$$\hat{\bar{L}} = \bar{q}S\left(\hat{C}_{\bar{L}_0}(\alpha,\beta,\delta_e) + \hat{C}_{\bar{L}_p}(\alpha,\beta)\frac{pb}{2V} + \hat{C}_{\bar{L}_r}(\alpha,\beta)\frac{rb}{2V} + \hat{C}_{\bar{L}_{\delta_e}}(\alpha,\beta)\delta_e + \hat{C}_{\bar{L}_{\delta_a}}(\alpha,\beta)\delta_a + \hat{C}_{\bar{L}_{\delta_r}}(\alpha,\beta)\delta_r\right)$$
$$\hat{\bar{M}} = \bar{q}S\left(\hat{C}_{\bar{M}_0}(\alpha,\beta) + \hat{C}_{\bar{M}_q}(\alpha)\frac{q\bar{c}}{2V} + \hat{C}_{\bar{M}_{\delta_e}}(\alpha,\beta)\delta_e\right) \tag{46}$$
$$\hat{\bar{N}} = \bar{q}S\left(\hat{C}_{\bar{N}_0}(\alpha,\beta,\delta_e) + \hat{C}_{\bar{N}_p}(\alpha,\beta)\frac{pb}{2V} + \hat{C}_{\bar{N}_r}(\alpha,\beta)\frac{rb}{2V} + \hat{C}_{\bar{N}_{\delta_e}}(\alpha,\beta)\delta_e + \hat{C}_{\bar{N}_{\delta_a}}(\alpha,\beta)\delta_a + \hat{C}_{\bar{N}_{\delta_r}}(\alpha,\beta)\delta_r\right)$$

Note that these approximations do not account for asymmetric failures that will introduce coupling of the longitudinal and lateral motions of the aircraft. If a failure occurs that introduces a parameter dependency that is not included in the approximation, stability can no longer be guaranteed. It is possible to include extra cross-coupling terms, but this is beyond the scope of this paper. The total nonlinear function approximations are divided into simpler linear-in-the-parameter nonlinear coefficient approximations: for example,

$$\hat{C}_{L_0}(\alpha,\beta) = \varphi^T_{C_{L_0}}(\alpha,\beta)\hat{\theta}_{C_{L_0}} \tag{47}$$

where the unknown parameter vector $\hat{\theta}_{C_{L_0}}$ contains the network weights (i.e., the unknown parameters), and $\varphi_{C_{L_0}}$ is a regressor vector containing the B-spline basis functions [29]. All other coefficient estimates are defined in similar fashion. In this case a two-dimensional network is used with input nodes for α and β. Different scheduling parameters can be selected for each unknown coefficient. In this study we use third-order B-splines spaced 2.5 deg and up to three scheduling variables, depending on the coefficient: α, β and δ_e. With these approximators, a sufficient model accuracy was obtained. Following the notation of Eq. (47), we can write the estimates of the aerodynamic forces and moments as

$$\hat{L} = \Phi^T_L(\alpha,\beta,\delta_e)\hat{\Theta}_L, \qquad \hat{\bar{L}} = \Phi^T_{\bar{L}}(\alpha,\beta,\delta_e)\hat{\Theta}_{\bar{L}}$$
$$\hat{Y} = \Phi^T_Y(\alpha,\beta,\delta_e)\hat{\Theta}_Y, \qquad \hat{\bar{M}} = \Phi^T_{\bar{M}}(\alpha,\beta,\delta_e)\hat{\Theta}_{\bar{M}} \tag{48}$$
$$\hat{D} = \Phi^T_D(\alpha,\beta,\delta_e)\hat{\Theta}_D, \qquad \hat{\bar{N}} = \Phi^T_{\bar{N}}(\alpha,\beta,\delta_e)\hat{\Theta}_{\bar{N}}$$

which is a notation equivalent to the one used in Eq. (44). Therefore, the update laws equation (43) can be used adapt the B-spline network weights. However, the update laws have not yet been robustified against nonparametric uncertainties such as 1) low-frequency unmodeled dynamics (e.g., structural vibrations) 2) measurement noise, 3) computational round-off errors and sampling delays, and 4) time variations of the unknown parameters, which can result in parameter drift. There are two categories of approaches for preventing parameter drift: those that prevent the parameter estimates from drifting to infinity directly (e.g., parameter projection or leakage terms) and those that stop the adaptation process when the training error is very small (e.g., dead zones [40,42]). In this paper dead zones and e modification are used to protect the estimated parameters from drifting.

V. Simulation Results

This section presents the simulation results from the application of the flight-path controller developed in the previous sections to the

Table 2 Maneuver 1 at flight condition 1: mean absolute values of the tracking errors and control inputs

Case	$(z_{01}, z_{02}, z_{03})^{\mathrm{MAV}}$, m	$(\delta_e, \delta_a, \delta_r)^{\mathrm{MAV}}$, deg	T^{MAV}, N
Nominal	(0.33,0.24,0.24)	(4.63, 0.12, 0.10)	$5.59e+04$
+30% uncertainty	(4.56,3.75,1.07)	(4.59, 0.13, 0.11)	$5.57e+04$
−30% uncertainty	(5.15,3.88,1.10)	(4.68, 0.16, 0.11)	$5.62e+04$
+10% deg, locked left aileron	(0.39,0.32,0.78)	(4.63, 0.56, 0.74)	$5.59e+04$
−10% deg, locked left aileron	(0.31,0.25,1.12)	(4.63, 0.46, 1.16)	$5.59e+04$

Table 3 Maneuver 1 at flight condition 2: mean absolute values of the tracking errors and control inputs

Case	$(z_{01}, z_{02}, z_{03})^{\mathrm{MAV}}$, m	$(\delta_e, \delta_a, \delta_r)^{\mathrm{MAV}}$, deg	T^{MAV}, N
Nominal	(0.30,0.23,0.21)	(3.97, 0.14, 0.21)	$3.14e+04$
+30% uncertainty	(1.55,1.33,0.41)	(3.96, 0.15, 0.23)	$3.14e+04$
−30% uncertainty	(2.01,1.53,0.52)	(3.98, 0.15, 0.20)	$3.14e+04$
+10% deg, locked left aileron	(0.36,0.33,0.72)	(3.97, 0.25, 1.20)	$3.14e+04$
−10% deg, locked left aileron	(0.30,0.28,1.01)	(3.96, 0.40, 1.52)	$3.14e+04$

Table 4 Maneuver 1 at flight condition 3: mean absolute values of the tracking errors and control inputs

Case	$(z_{01}, z_{02}, z_{03})^{\mathrm{MAV}}$, m	$(\delta_e, \delta_a, \delta_r)^{\mathrm{MAV}}$, deg	T^{MAV}, N
Nominal	(0.33,0.22,0.27)	(3.37, 0.08, 0.08)	$4.41e+04$
+30% uncertainty	(2.01,1.43,0.61)	(3.40, 0.10, 0.08)	$4.44e+04$
−30% uncertainty	(2.16,1.49,0.77)	(3.38, 0.09, 0.08)	$4.41e+04$
+10% deg, locked left aileron	(0.32,0.33,0.29)	(3.38, 0.08, 0.09)	$4.41e+04$
−10% deg, locked left aileron	(0.34,0.24,0.30)	(3.38, 0.08, 0.09)	$4.41e+04$

high-fidelity, six-degree-of-freedom F-16 model of Sec. II. Both the control law and the aircraft model are written as *C* S-functions in MATLAB/Simulink. The simulations are performed at three different starting flight conditions with the trim conditions: 1) $h = 5000$ m, $V = 200$ m/s, and $\alpha = \theta = 2.774$ deg; 2) $h = 0$ m, $V = 250$ m/s, and $\alpha = \theta = 2.406$ deg; and 3) $h = 2500$ m, $V = 150$ m/s, and $\alpha = \theta = 0.447$ deg; where h is the altitude of the aircraft, and all other trim states are equal to zero.

Furthermore, two maneuvers are considered: 1) a climbing helical path and 2) a reconnaissance and surveillance maneuver. The latter maneuver involves turns in both directions and some altitude changes. The simulations of both maneuvers last 300 s. The reference trajectories are generated with second-order linear filters to ensure smooth trajectories. To evaluate the effectiveness of the online model identification, all maneuvers will also be performed with a $\pm 30\%$ deviation in all aerodynamic stability and control derivatives used by

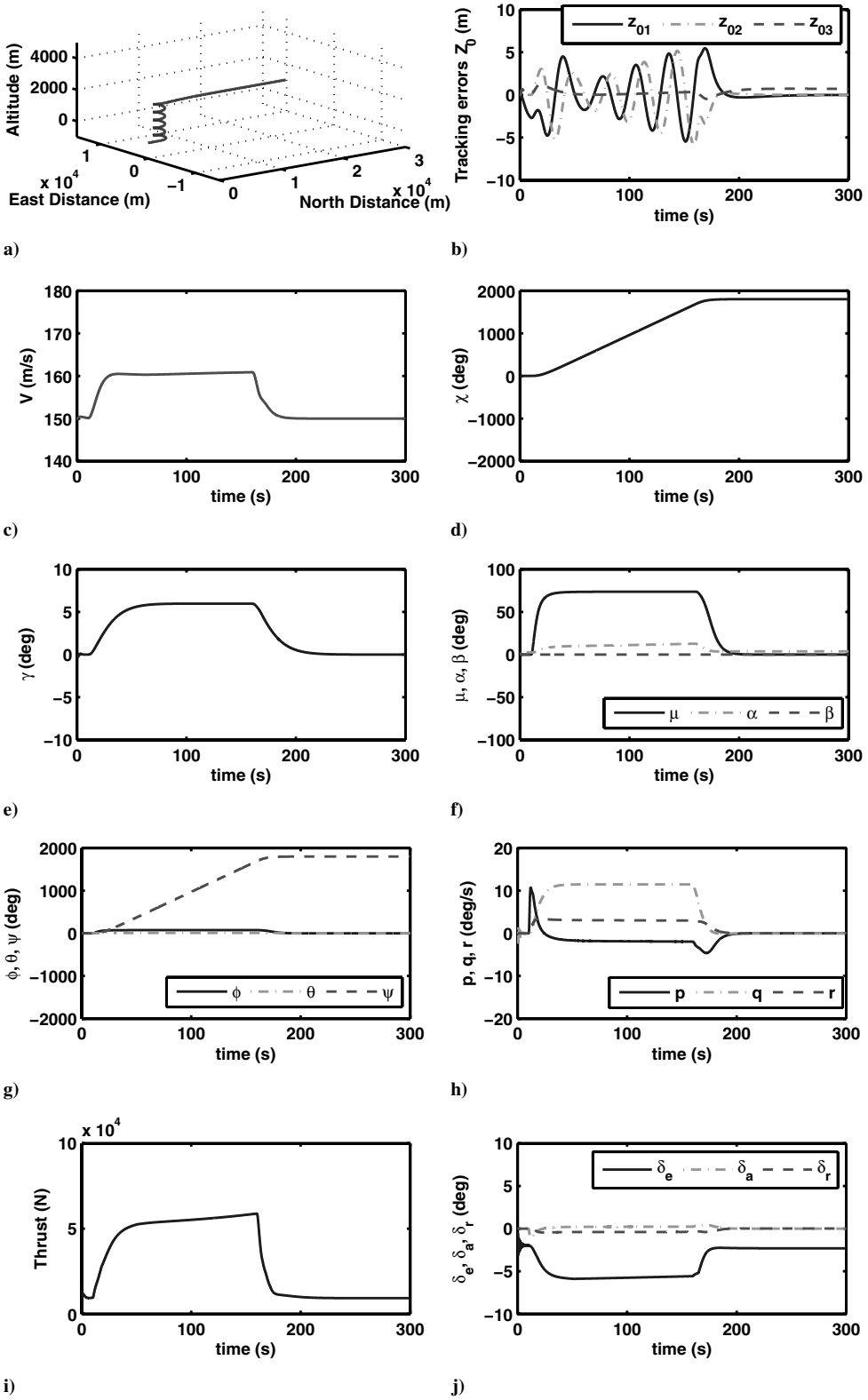

Fig. 4 Maneuver 1: climbing helical path performed at flight condition 2 with +30% uncertainty in the aerodynamic coefficients.

the controller (i.e., it is assumed that the onboard model is very inaccurate). Finally, the same maneuvers are also simulated with a lockup at ± 10 deg of the left aileron.

A. Controller Parameter Tuning

We start with the selection of the gains of the static control law and the bandwidths of the command filters. Lyapunov stability theory only requires the control gains to be larger than zero, but it is natural to select the largest gains of the inner loop. Larger gains will, of course, result in smaller tracking errors, but at the cost of more control effort. It is possible to derive certain performance bounds that can serve as guidelines for tuning (see, for example, [43,44]). However, getting the desired closed-loop response is still an extensive trial-and-error procedure. The control gains were selected as $c_{01} = 0.1$, $c_{02} = 1.10^{-5}$, $c_{03} = 0.5$, $c_{11} = 0.01$, $c_{12} = 2.5$, $c_{13} = 0.5$, $C_2 = \text{diag}(1, 1, 1)$, and $C_3 = \text{diag}(2, 2, 2)$.

The bandwidths of the command filters for the actual control variables δ_e, δ_a, and δ_r are chosen to be equal to the bandwidths of the actuators, which are given in [29]. The outer-loop filters have the

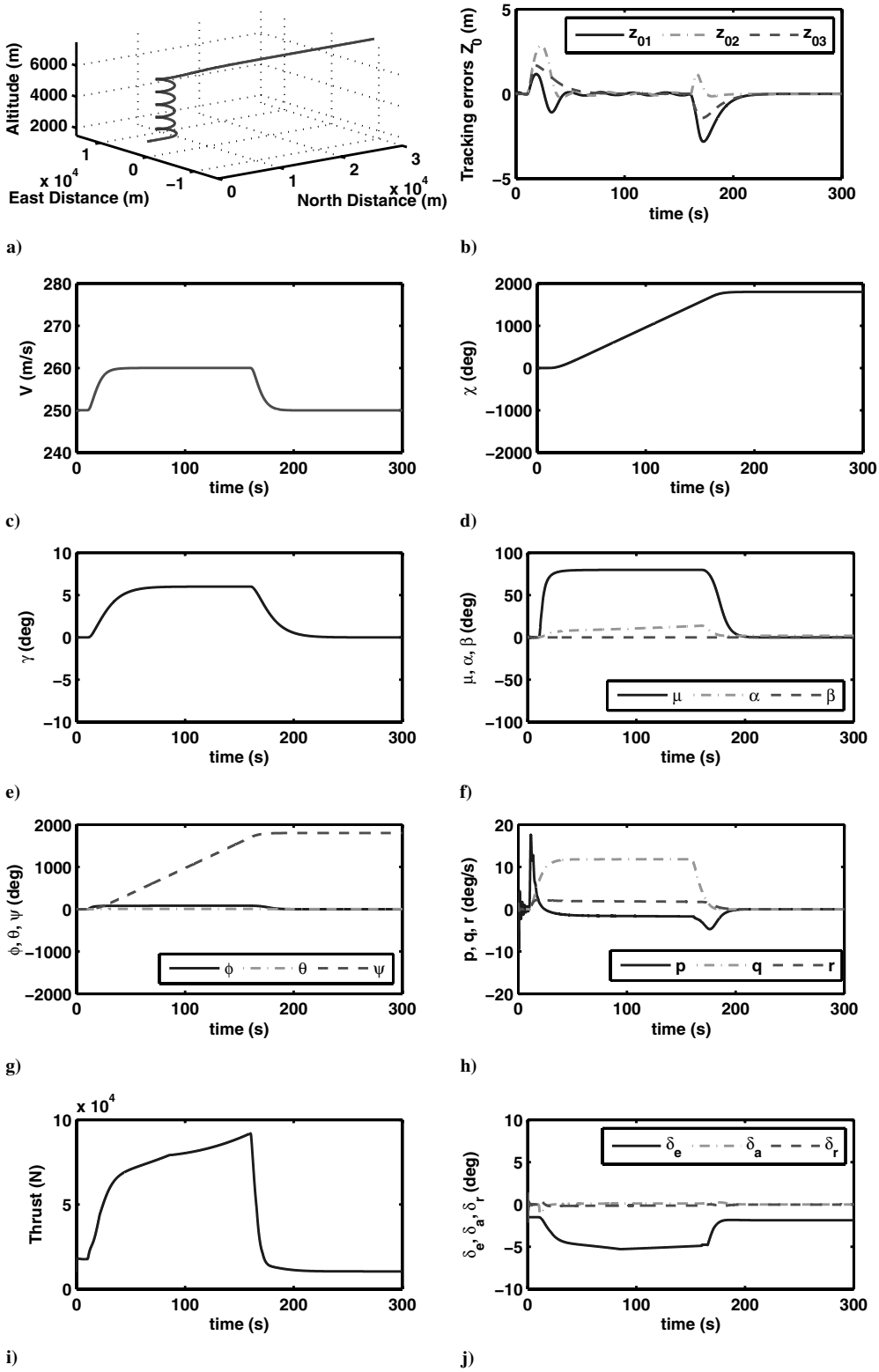

Fig. 5 Maneuver 1: climbing helical path performed at flight condition 3 with left aileron locked at −10 deg.

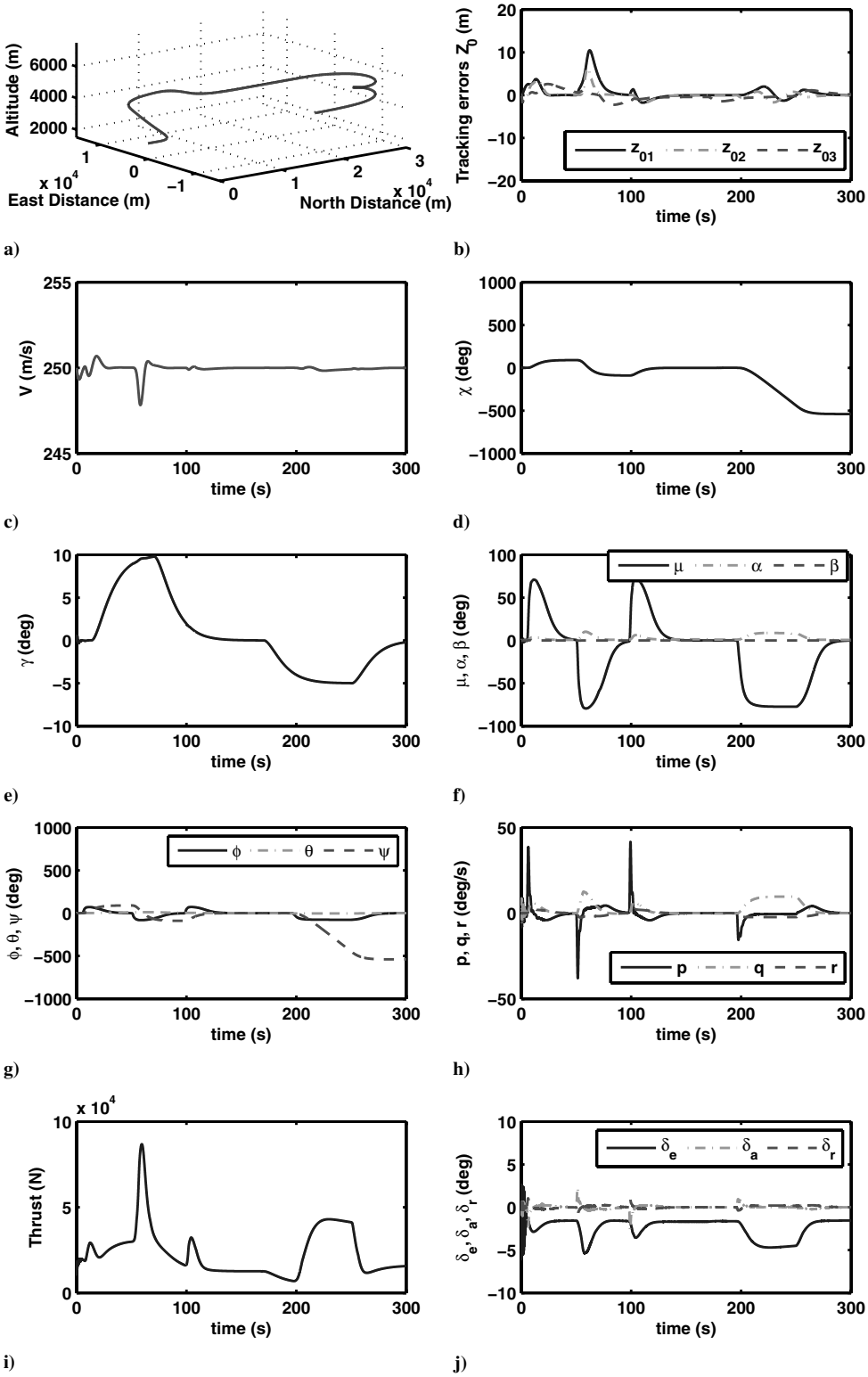

Fig. 6 Maneuver 2: reconnaissance and surveillance performed at flight condition 3 with −30% uncertainty in the aerodynamic coefficients.

Table 5 Maneuver 2 at flight condition 3: mean absolute values of the tracking errors and control inputs

Case	$(z_{01}, z_{02}, z_{03})^{\mathrm{MAV}}$, m	$(\delta_e, \delta_a, \delta_r)^{\mathrm{MAV}}$, deg	T^{MAV}, N
Nominal	(0.49,0.40,0.56)	(2.39, 0.12, 0.12)	$2.33e+04$
+30% uncertainty	(0.97,0.78,0.54)	(2.39, 0.12, 0.13)	$2.33e+04$
−30% uncertainty	(0.97,0.56,0.85)	(2.40, 0.13, 0.12)	$2.33e+04$
+10% deg, locked left aileron	(0.48,0.40,0.58)	(2.39, 0.12, 0.13)	$2.33e+04$
−10% deg, locked left aileron	(0.49,0.40,0.56)	(2.40, 0.13, 0.13)	$2.33e+04$

Table 6 Maneuver 2 at flight condition 1: Mean absolute values of the tracking errors and control inputs

Case	$(z_{01}, z_{02}, z_{03})^{\mathrm{MAV}}$, m	$(\delta_e, \delta_a, \delta_r)^{\mathrm{MAV}}$, deg	T^{MAV}, N
Nominal	(0.42,0.39,0.46)	(3.17, 0.16, 0.13)	$2.25e+04$
+30% uncertainty	(2.69,2.30,1.13)	(3.16, 0.16, 0.14)	$2.25e+04$
−30% uncertainty	(3.02,2.40,1.12)	(3.19, 0.18, 0.14)	$2.25e+04$
+10% deg, locked left aileron	(0.43,0.40,0.45)	(3.17, 0.17, 0.16)	$2.25e+04$
−10% deg, locked left aileron	(0.42,0.39,0.46)	(3.17, 0.17, 0.15)	$2.25e+04$

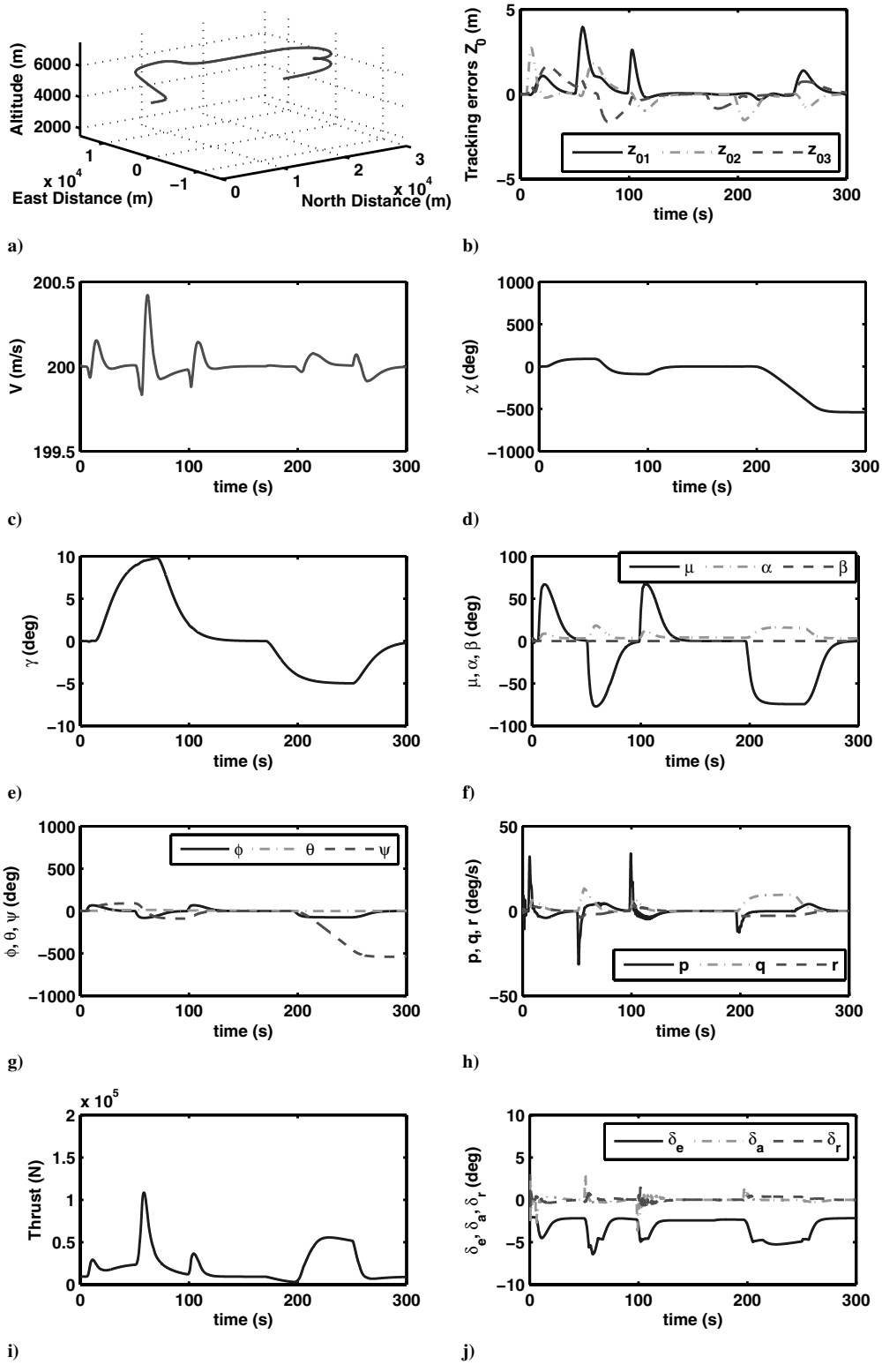

Fig. 7 Maneuver 2: reconnaissance and surveillance path performed at flight condition 1 with left aileron locked at +10 deg.

Table 7 Maneuver 2 at flight condition 2: mean absolute values of the tracking errors and control inputs

Case	$(z_{01}, z_{02}, z_{03})^{\mathrm{MAV}}$, m	$(\delta_e, \delta_a, \delta_r)^{\mathrm{MAV}}$, deg	T^{MAV}, N
Nominal	(0.58,0.49,0.34)	(2.95, 0.18, 0.21)	$1.62e+04$
+30% uncertainty	(1.27,1.10,0.48)	(2.95, 0.19, 0.22)	$1.62e+04$
−30% uncertainty	(1.73,1.24,0.55)	(2.97, 0.19, 0.21)	$1.61e+04$
+10% deg, locked left aileron	(0.58,0.50,0.35)	(2.95, 0.20, 0.22)	$1.62e+04$
−10% deg, locked left aileron	(0.59,0.51,0.34)	(2.95, 0.22, 0.22)	$1.62e+04$

smallest bandwidths. The selection of the other bandwidths is again trial and error. A higher bandwidth in a certain feedback loop will result in more aggressive commands to the next feedback loop. All damping ratios are equal to 1.0. It is possible to add magnitude and rate limits to each of the filters. In this study magnitude limits on the aerodynamic roll angle μ and the flight-path angle γ are used to avoid singularities in the control laws. Rate and magnitude limits equal to those of the actuators are enforced on the actual control variables. The selected command-filter parameters can be found back in Table 1. As soon as the controller gains and command-filter parameters have been defined, the update law gains can be selected. Again, the theory only requires that the gains should be larger than zero. Larger update gains means higher learning rates and thus more rapid changes in the B-spline network weights.

B. Maneuver 1: Upward Spiral

In this section the results of the numerical simulations of the first test maneuver, the climbing helical path, are discussed. For each of the three flight conditions, five cases are considered: nominal, the aerodynamic stability and control derivatives used in the control law perturbed with +30% and with −30% with respect to the real values of the model, a lockup of the left aileron at +10 deg, and a lockup at −10 deg. No actuator sensor information is used. In Fig. 3 the results are plotted of the simulation without uncertainty, starting at flight condition 1. The maneuver involves a climbing spiral to the left with an increase in airspeed. It can be seen that the control law manages to track the reference signal very well and closed-loop tracking is achieved. The sideslip angle does not become any larger than ±0.02 deg. The aerodynamic roll angle does reach the limit set by the command filter, but this has no consequences for the performance. The use of dead zones ensures that the parameter update laws are indeed not updating during this maneuver without any uncertainties. The responses at the two other flight conditions are virtually the same, although less thrust is needed due to the lower altitude of flight condition 2 and the lower airspeed of flight condition 3. The other control surfaces are also more efficient. This is illustrated in Tables 2–4, in which the mean absolute values (MAVs) of the outer-loop tracking errors, control-surface deflections, and thrust can be found. Plots of the parameter-estimation errors are not included. However, the errors converge to constant values, but not to zero, as is common with Lyapunov-based update laws [29,45].

The response of the closed-loop system during the same maneuver starting at flight condition 1, but with +30% uncertainty in the aerodynamic coefficients, is shown in Fig. 4. It can be observed that the tracking errors of the outer loop are now much larger, but in the end, the steady-state tracking error converges to zero. The sideslip angle still remains within 0.02 deg. Some small oscillations are visible in Fig. 4j, but these stay well within the rate and magnitude limits of the actuators. In Tables 2–4 the MAVs of the tracking errors and control inputs are shown for all flight conditions. As was already seen in the plots, the average tracking errors increase, but the magnitude of the control inputs stays approximately the same. The same simulations have been performed for a −30% perturbation in the stability and control derivatives used by the control law, and the results are also shown in the tables. It appears that underestimated initial values of the unknown parameters lead to larger tracking errors than overestimates for this maneuver.

Finally, the maneuver is performed with the left aileron locked at ±10 deg [i.e., $\delta_a^{\mathrm{damaged}} = 0.5(\delta_a \pm 10\pi/180)$]. Figure 5 shows the response at flight condition 3 with the aileron locked at −10 deg. Except for some small oscillations in the response of roll rate p, there is no real change in performance visible; this is confirmed by the numbers of Table 4. However, from Tables 2 and 3 we observe that aileron and rudder deflections become larger with both locked aileron failure cases, whereas tracking performance hardly declines.

C. Maneuver 2: Reconnaissance

The second maneuver, called reconnaissance and surveillance, involves turns in both directions and altitude changes, but airspeed is kept constant. Plots of the simulation at flight condition 3 with −30% uncertainty are shown in Fig. 6. Tracking performance is again excellent and the steady-state tracking errors converge to zero. There are some small oscillations in the rudder deflection, but these are within the limits of the actuator. We compare the MAVs of the tracking errors and control inputs with those for the nominal case in Table 5 and observe that the average tracking errors have not increased much for this case. The degradation of performance for the uncertainty cases is somewhat worse at the other two flight conditions, as can be seen in Tables 6 and 7. The sideslip angle always remains within 0.05 deg for all flight conditions and uncertainties. Corresponding with the results of maneuver 1, overestimation of the unknown parameters again leads to smaller tracking errors.

Simulations of maneuver 2 with the locked aileron are also performed. Figure 7 shows the results for flight condition 1 with a locked aileron at +10 deg. Some very small oscillations are again visible in the roll rate, aileron, and rudder responses, but tracking performance is good and steady-state convergence is achieved. Table 6 confirms that the results of the simulations with actuator failure hardly differ from the nominal case. There is only a small increase in the use of the lateral control surfaces. The same holds at the other flight conditions, as can be seen in Tables 5 and 7.

VI. Conclusions

In this paper a nonlinear adaptive flight-path control system is designed for a high-fidelity F-16 model. The controller is based on a backstepping approach with four feedback loops that are designed using a single control Lyapunov function to guarantee stability. The uncertain aerodynamic forces and moments of the aircraft are approximated online with B-spline neural networks for which the weights are adapted by Lyapunov-based update laws. Numerical simulations of two test maneuvers were performed at several flight conditions to verify the performance of the control law. Actuator failures and uncertainties in the stability and control derivatives are introduced to evaluate the parameter-estimation process. The results show that trajectory control can still be accomplished with these uncertainties and failures, and good tracking performance is maintained. Compared with other Lyapunov-based trajectory control designs, the approach is much simpler to apply and the online estimation process is more robust to saturation effects. Future studies will focus on the actual trajectory generation and the extension to formation-flying control.

References

[1] Clough, B. T., "Unmanned Aerial Vehicles: Autonomous Control Challenges, a Researchers Perspective," *Journal of Aerospace Computing, Information, and Communication*, Vol. 2, No. 8, 2005, pp. 327–347.
doi:10.2514/1.5588

[2] Wegener, S., Sullivan, D., Frank, J., and Enomoto, F., "UAV Autonomous Operations for Airborne Science Missions," AIAA 3rd "Unmanned Unlimited" Technical Conference, Workshop and Exhibit, AIAA Paper 2004-6416, 2004.

[3] Papadales, B., and Downing, M., "UAV Science Missions: A Business Perspective," Infotech@Aerospace, AIAA Paper 2005-6922, 2005.

[4] Tsach, S., Chemla, J., and Penn, D., "UAV Systems Development in IAI-Past, Present and Future," 2nd AIAA "Unmanned Unlimited" Systems, Technologies, and Operations-Aerospace Land, and Sea Conference, AIAA Paper 2003–6535, Sept. 20032003.

[5] Kaminer, I., Pascoal, A., Hallberg, E., and Silvestre, C., "Trajectory Tracking for Autonomous Vehicles: An Integrated Approach to Guidance and Control," *Journal of Guidance, Control, and Dynamics*, Vol. 21, No. 1, 1998, pp. 29–38. doi:10.2514/2.4229

[6] Boyle, D. P., and Chamitof, G. E., "Autonomous Maneuver Tracking for Self-Piloted Vehicles," *Journal of Guidance, Control, and Dynamics*, Vol. 22, No. 1, 1999, pp. 58–67. doi:10.2514/2.4371

[7] Singh, S. N., Steinberg, M. L., and Page, A. B., "Nonlinear Adaptive and Sliding Mode Flight Path Control of F/A-18 Model," *IEEE Transactions on Aerospace and Electronic Systems*, Vol. 39, No. 4, 2003, pp. 1250–1262. doi:10.1109/TAES.2003.1261125

[8] Ren, W., and Beard, R. W., "Trajectory Tracking for Unmanned Air Vehicles with Velocity and Heading Rate Constraints," *IEEE Transactions on Control Systems Technology*, Vol. 12, No. 5, 2004, pp. 706–716. doi:10.1109/TCST.2004.826956

[9] Ren, W., and Atkins, E., "Nonlinear Trajectory Tracking for Fixed Wing UAVs via Backstepping and Parameter Adaptation," AIAA Guidance, Navigation, and Control Conference and Exhibit, AIAA Paper 2005-6196, Aug. 2005.

[10] No, T. S., Min, B. M., Stone, R. H., and K. C. Wong, J. E., "Control and Simulation of Arbitrary Flight Trajectory-Tracking," *Control Engineering Practice*, Vol. 13, No. 5, 2005, pp. 601–612. doi:10.1016/j.conengprac.2004.05.002

[11] Kaminer, I., Yakimenko, O., Dobrokhodov, V., Pascoal, A., Hovakimyan, N., Cao, C., Young, A., and Patel, V., "Coordinated Path Following for Time-Critical Missions of Multiple UAVs via L1 Adaptive Output Feedback Controllers," AIAA Guidance, Navigation, and Control Conference and Exhibit, AIAA Paper 2007-6409, 2007.

[12] Pachter, M., D'Azzo, J. J., and J. L. Dargan, "Automatic Formation Flight Control," *Journal of Guidance, Control, and Dynamics*, Vol. 17, No. 6, 1994, pp. 1380–1383.

[13] Proud, A. W., Pachter, M., and D'Azzo, J. J., "Close Formation Flight Control," AIAA Guidance, Navigation, and Control Conference, AIAA Paper 1999-4207, 1999.

[14] Fujimori, A., Kurozumi, M., Nikiforuk, P. N., and Gupta, M. M., "Flight Control Design of an Automatic Landing Flight Experiment Vehicle," *Journal of Guidance, Control, and Dynamics*, Vol. 23, No. 2, 2000, pp. 373–376. doi:10.2514/2.4536

[15] Singh, S. N., Chandler, P., Schumacher, C., Banda, S., and Pachter, M., "Adaptive Feedback Linearizing Nonlinear Close Formation Control of UAVs," *American Control Conference*, Inst. of Electrical and Electronics Engineers, Piscataway, NJ, June 2000, pp. 854–858.

[16] Pachter, M., D'Azzo, J. J., and Proud, A. W., "Tight Formation Control," *Journal of Guidance, Control, and Dynamics*, Vol. 24, No. 2, 2001, pp. 246–254. doi:10.2514/2.4735

[17] Wang, J., Patel, V., Cao, C., Hovakimyan, N., and Lavretsky, E., "Novel L1 Adaptive Control Methodology for Aerial Refueling with Guaranteed Transient Performance," *Journal of Guidance, Control, and Dynamics*, Vol. 31, No. 1, 2008, pp. 182–193. doi:10.2514/1.31199

[18] Healy, A., and Liebard, D., "Multivariable Sliding Mode Control for Autonomous Diving and Steering of Unmanned Underwater Vehicles," *IEEE Journal of Oceanic Engineering*, Vol. 18, No. 3, 1993, pp. 327–339. doi:10.1109/JOE.1993.236372

[19] Narasimhan, M., Dong, H., Mittal, R., and Singh, S. N., "Optimal Yaw Regulation and Trajectory Control of Biorobotic AUV Using Mechanical Fins Based on CFD Parametrization," *Journal of Fluids Engineering*, Vol. 128, No. 4, 2006, pp. 687–698. doi:10.1115/1.2201634

[20] Kannelakopoulos, I., Kokotović, P. V., and Morse, A. S., "Systematic Design of Adaptive Controllers for Feedback Linearizable Systems," *IEEE Transactions on Automatic Control*, Vol. 36, No. 11, Nov. 1991, pp. 1241–1253. doi:10.1109/9.100933

[21] Krstić, M., Kanellakopoulos, I., and Kokotović, P. V., "Adaptive Nonlinear Control Without Overparametrization," *Systems and Control Letters*, Vol. 19, Sept. 1992, pp. 177–185. doi:10.1016/0167-6911(92)90111-5

[22] Singh, S. N., and Steinberg, M., "Adaptive Control of Feedback Linearizable Nonlinear Systems With Application to Flight Control," AIAA Guidance, Navigation, and Control Conference, AIAA Paper 1996-3771, July 1996.

[23] Härkegård, O., "Backstepping and Control Allocation with Applications to Flight Control," Ph.D. Thesis, Linköping Univ., Linköping, Sweden, 2003.

[24] Farrell, J., Polycarpou, M., and Sharma, M., "Adaptive Backstepping with Magnitude, Rate, and Bandwidth Constraints: Aircraft Longitude Control," *American Control Conference*, American Control Conference Council, Evanston, IL, 2003, pp. 3898–3903.

[25] Kim, S. H., Kim, Y. S., and Song, C., "A Robust Adaptive Nonlinear Control Approach to Missile Autopilot Design," *Control Engineering Practice*, Vol. 12, No. 2, 2004, pp. 149–154. doi:10.1016/S0967-0661(03)00016-9

[26] Shin, D. H., and Kim, Y., "Reconfigurable Flight Control System Design Using Adaptive Neural Networks," *IEEE Transactions on Control Systems Technology*, Vol. 12, No. 1, Jan. 2004, pp. 87–100. doi:10.1109/TCST.2003.821957

[27] Farrell, J., Sharma, M., and Polycarpou, M., "Backstepping Based Flight Control with Adaptive Function Approximation," *Journal of Guidance, Control, and Dynamics*, Vol. 28, No. 6, Jan. 2005, pp. 1089–1102. doi:10.2514/1.13030

[28] Sonneveldt, L., Chu, Q. P., and Mulder, J. A., "Constrained Adaptive Backstepping Flight Control: Application to a Nonlinear F-16/MATV Model," AIAA Guidance, Navigation, and Control Conference and Exhibit, AIAA Paper 2006-6413, Aug. 2006.

[29] Sonneveldt, L., Chu, Q. P., and Mulder, J. A., "Nonlinear Flight Control Design Using Constrained Adaptive Backstepping," *Journal of Guidance, Control, and Dynamics*, Vol. 30, No. 2, Mar.–Apr. 2007, pp. 322–336. doi:10.2514/1.25834

[30] Yip, P.-C. P., "Robust and Adaptive Nonlinear Control Using Dynamic Surface Controller with Applications to Intelligent Vehicle Highway Systems," Ph.D. Thesis, Univ. of California at Berkeley, Berkeley, CA, 1997.

[31] Cheng, K. W. E., Wang, H., and Sutanto, D., "Adaptive B-Spline Network Control for Three-Phase PWM AC-DC Voltage Source Converter," *IEEE 1999 International Conference on Power Electronics and Drive Systems*, Inst. of Electrical and Electronics Engineers, Piscataway, NJ, 1999, pp. 467–472.

[32] Ward, D. G., Sharma, M., Richards, N. D., , and Mears, M., "Intelligent Control of Un-Manned Air Vehicles: Program Summary and Representative Results," 2nd AIAA Unmanned Unlimited Systems, Technologies and Operations Aerospace, Land and Sea, AIAA Paper 2003-6641, 2003.

[33] Nguyen, L. T., Ogburn, M. E., Gilbert, W. P., Kibler, K. S., Brown, P. W., and Deal, P. L., "Simulator Study of Stall Post-Stall Characteristics of a Fighter Airplane with Relaxed Longitudinal Static Stability," NASA Langley Research Center, Hampton, VA, 1979.

[34] Lewis, B. L., and Stevens, F. L., *Aircraft Control and Simulation*, Wiley, New York, 1992, pp. 1–54, 110–115.

[35] Cook, M. V., *Flight Dynamics Principles*, Butterworth-Heinemann, London, 1997, pp. 11–29.

[36] Swaroop, D., Gerdes, J. C., Yip, P. P., and Hedrick, J. K., "Dynamic Surface Control of Nonlinear Systems," *Proceedings of the American Control Conference*, 1997.

[37] Kanayama, Y. J., Kimura, Y., Miyazaki, F., and Noguchi, T., "A Stable Tracking Control Method for an Autonomous Mobile Robot," *IEEE International Conference on Robotics and Automation*, Inst. of Electrical and Electronics Engineers, Piscataway, NJ, 1990, pp. 384–389.

[38] Enns, D. F., "Control Allocation Approaches," AIAA Guidance, Navigation, and Control Conference and Exhibit, AIAA Paper 1998-4109, Aug. 1998.

[39] Durham, W. C., "Constrained Control Allocation," *Journal of Guidance, Control, and Dynamics*, Vol. 16, No. 4, 1993, pp. 717–725. doi:10.2514/3.21072

[40] Ioannou, P. A., and Sun, J., *Stable and Robust Adaptive Control*, Prentice–Hall, Englewood Cliffs, NJ, 1995, pp. 555–575.

[41] Babuška, R., *Fuzzy Modeling for Control*, Kluwer Academic, Norwell, MA, 1998, pp. 49–52.

[42] Karason, S. P., and Annaswamy, A. M., "Adaptive Control in the Presence of Input Constraints," *IEEE Transactions on Automatic Control*, Vol. 39, No. 11, 1994, pp. 2325–2330. doi:10.1109/9.333787

[43] Krstić, M., Kokotović, P. V., and Kanellakopoulos, I., "Transient Performance Improvement with a New Class of Adaptive Controllers," *Systems and Control Letters*, Vol. 21, No. 6, 1993, pp. 451–461. doi:10.1016/0167-6911(93)90050-G

[44] Sonneveldt, L., van Oort, E. R., Chu, Q. P., and Mulder, J. A., "Comparison of Inverse Optimal and Tuning Functions Designs for Adaptive Missile Control," AIAA Guidance, Navigation, and Control Conference and Exhibit, AIAA Paper 2007-6675, 2007.

[45] Page, A. B., and Steinberg, M. L., "Effects of Control Allocation Algorithms on a Nonlinear Adaptive Design," *AIAA Guidance, Navigation, and Control Conference and Exhibit*, AIAA, Reston, VA, Aug. 1999, pp. 1664–1674; also AIAA Paper 1999-4282.